ELSEVIER

International Journal of Heat and Fluid Flow 21 (2000) 576–581

International Journal of
HEAT AND
FLUID FLOW

www.elsevier.com/locate/ijhff

Statistical analysis on wall shear stress of turbulent boundary layer in a channel flow using micro-shear stress imager

Norimasa Miyagi [a,*], Motoaki Kimura [a], Hideo Shoji [a], Atsusi Saima [a], Chih-Ming Ho [b], Steve Tung [b], Yu-Chong Tai [c]

[a] *Department of Mechanical Engineering, College of Science and Technology, Nihon University, 1-8 Kanda Surugadai, Ciyoda-ku, Tokyo 101-8308, Japan*

[b] *Mechanical and Aerospace Engineering Department, University of California, Los Angeles, Los Angeles, CA 90095, USA*

[c] *Division of Engineering and Applied Science, California Institute of Technology, Pasadena, CA 91125, USA*

Abstract

Measurements of wall shear stress of turbulent boundary layers in the channel flow were carried out using a micro-electro-mechanical-system (MEMS)-based micro-shear stress imaging chip. The study was carried out in a turbulent channel flow facility. One array of 25 micro-shear stress sensors in the chip that covers a length of 7.5 mm is used to measure the instantaneous span-wise distribution of the surface shear stress. The characteristics of high shear stress area (streaks) were described with statistics. Based on the measurement, the physical quantities associated with the high shear stress streaks, such as their length, width with the high shear stress level, were obtained. To further explore the relationship between the shear stress slope and the peak shear stress, the probability density function (PDF) of the ratio of peak shear stress to shear stress slope at different Reynolds number *Re* is examined. As for the distribution of PDF, it was found that the distribution concentrated towards a certain value in each *Re*. This result is extremely important because it points to the possibility of predicting the peak shear stress level based on the shear stress distribution at the leading edge of the streaks.

1. Introduction

The presence of near-wall streak structure in a turbulent boundary layer has been observed for many years in flow visualization and experimental investigation (Kline et al., 1967; Kim et al., 1971; Falco, 1980; Cantwell, 1981; Head and Bandyopadhyay, 1981; Smith and Metzler, 1983). At high Reynolds number, *Re*, these streaks are typically very small in size and cannot be properly resolved by traditional measuring techniques. Numerical simulations indicate that the streaks are associated with streamwise vortices in the viscous sub-layer. The rotational motion of these vortices imposes high fluctuating surface shear stress on the wall (Kim et al., 1987).

There have been many measurement techniques for measuring shear stress. The hot-film technique and its variants have been widely used for the detailed investigation of fluctuating wall shear stress (Alfreadsson et al., 1988; Bruun, 1995). The direction sensitive laser Doppler anemometer is a candidate, which enables to evaluate both magnitude and direction of the wall shear stress. An optical method proposed by Naqwi and Reynolds (1991) is supposed to be capable of measuring the wall shear stress with high spatial resolution. Irrespective of the instrument, the requirements of fine spatial resolution, fast frequency response, high sensitivity and convenience need to be satisfied for turbulent boundary layer research.

Recently, the availability of a new manufacturing process, micro-electro-mechanical-system (MEMS) technology, has offered the possibility of sensing and controlling the small near-wall streaks (Ho et al., 1997). A multidisciplinary research collaboration between UCLA and Caltech has been made to design and fabricate a large-scale distribution control system with integrated micro-machined transducer and microelectronic circuits for surface shear stress control in turbulent boundary layers (Tung et al., 1995, Ho et al., 1996). The principal aim is to develop a real-time micro-system that consists of a large number of shear stress sensors and actuators integrated with the neural network control circuit.

In this paper, our effort is directed to qualifying the characteristics of near-wall streaks and to provide a control guideline for the control system. First, this paper presents the micro-shear stress sensor and measurement. Secondly, the performance of a micro-shear stress sensor is compared with the existing experimental data. Thirdly, the characteristics and the several statistical results of shear stress streaks are presented, and the information of shear stress streaks is taken up for predicting the shear stress peak level with concrete numerical value.

* Corresponding author. Tel.: +81-3-3259-0750; fax: +81-3-3293-8254.

E-mail address: miyagi@st.mech.cst.nihon-u.ac.jp (N. Miyagi).

0142-727X/00/$ - see front matter
PII: S0142-727X(00)00047-3

2. Facility and micro-shear stress imaging chip

2.1. Micro-shear stress imaging chip

A micro-shear stress imaging chip, which is composed of multiple micro-shear stress sensors (Jiang et al., 1996), is exhibited in Fig. 1. Five rows of the micro-sensor were installed on the imaging chip, three of which contain 25 sensors each and two of which contain 5 sensors each. Within each array, the distance between sensors is 300 μm. The sensors are thermal types. Each micro-sensor consists of a 150 μm long, 3 μm wide, and 0.45 μm thick polysilicon resistor wire and a 2 μm deep vacuum cavity underneath. The purpose of the cavity is to reduce heat transfer from the resistor wire to the substrate and increase the sensitivity of the sensor (Huage et al., 1996). The sensors are connected to external constant temperature mode circuits.

Output signals from the anemometer circuits are digitized by a 64-channel ADC board in a Pentium 120 similar to a hot-wire anemometer. It is driven at an overheat ratio of 1.1. At a gain of 10, the sensitivity of the shear stress sensor is about 1 V/Pa with a frequency response of 25 kHz. The first array of 1–25 micro-shear stress sensors that covers a distance of 7.5 mm is used to measure the instantaneous span-wise distribution of the turbulent boundary surface shear stress.

2.2. Shear stress sensor calibration and temperature compensation

The heating power of a shear stress sensor operating in steady state can be correlated with wall shear stress τ as follows (Bruun, 1995):

$$i^2R^2 = (T_f - T)(A + B\tau^{1/3}), \tag{1}$$

where T_f and T are the temperature of the sensor and the measured fluid, respectively, R the resistance of the sensor, i the heating current going through the sensor, and A and B are calibration constants. In order to correlate the output voltage with the wall shear stress τ, two theoretical methods are used here. In the first method, τ in a fully developed turbulent flow of the channel is related to the stream-wise pressure gradient by

$$dP_x/dx = -\tau/h, \tag{2}$$

where P_x is the local pressure, x the stream-wise coordinate, and h is the half-height of the channel. The pressure drop and output voltage of the sensor were measured at different center velocities of the channel ranging from 10 to 20 m/s. If the temperature of the measured fluid T is constant, the wall shear stress can be directly related to the output voltage E_0 by a sixth-order polynomial with the data

$$\tau = a_0 + a_1E_0 + \cdots + a_6E_0^6, \tag{3}$$

where $a_0, a_1, a_2, \ldots, a_6$ are calibration constants. These constants were calibrated in the channel flow in a downstream region, where the turbulent flow was fully developed. In the second method, an empirical relationship between the Reynolds number and the wall shear stress in a fully developed channel flow is obtained (Hussain and Reynolds, 1970), by using

$$u_\tau/u_\infty = 0.1079Re^{-0.089} \tag{4}$$

and

$$\tau = u_\tau^2\rho, \tag{5}$$

where u_τ is the friction velocity, u_∞ the center velocity of the channel, Re is calculated using the mean centerline velocity, and ρ is the air density. We first measure the stream-wise pressure gradient and calculate τ by using Eq. (2). In addition, we use the second method given by Eqs. (4) and (5) to calculate the wall shear stress again. Good agreement is found between shear stress values calculated by both methods.

When the ambient fluid temperature, T, varies during the measurement, a thermal correction should be applied. To find out the correlation coefficient of the temperature compensation, previous micro-shear stress sensor versus fine thermocouple have been measured simultaneously in the channel flow at 10 m/s under the room temperature range of 19.0–22.0°C. The slope of the sensor output as a function of temperature is −310 mV/°C. Temperature compensation was achieved by collecting both ambient temperature and shear stress data first, then correcting accordingly with the software after the experiment.

2.3. Experimental setup

The study was carried out in a turbulent channel flow facility (Fig. 2(a)). The channel constructed of 13 mm Plexiglas, is 610 mm × 25.4 mm in cross-section and 4880 mm long. An

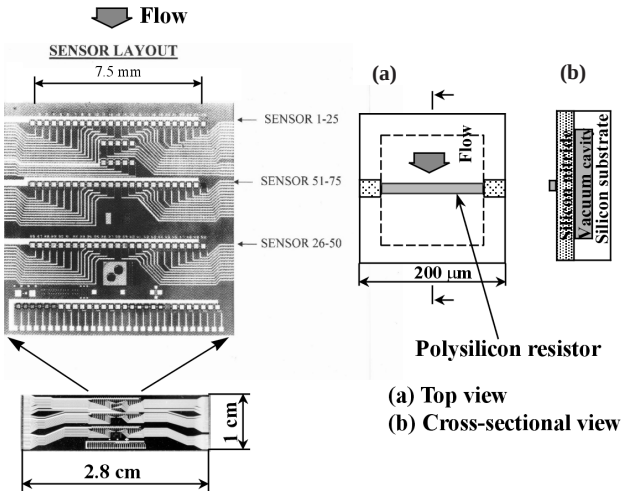

Fig. 1. Shear stress imaging chip.

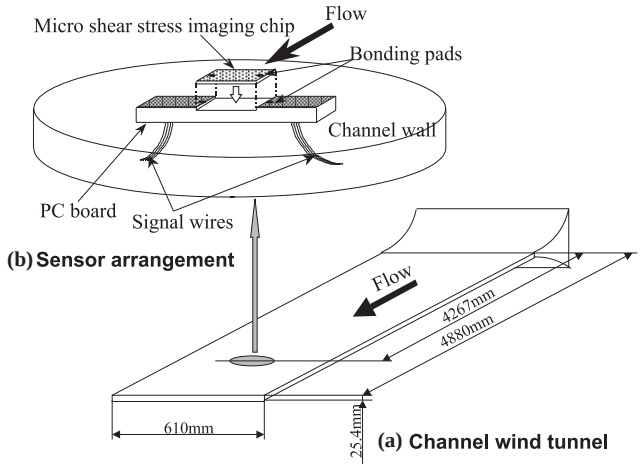

Fig. 2. Sensor arrangement.

axial blower controlled by a DC power supply generates the air flow in the channel. Previous hot-wire measurements indicate that the channel flow, with a centerline velocity of 10 m/s, consists of a laminar entrance flow and a fully developed turbulent flow in the downstream half of the channel. The micro-shear stress imaging chip was packaged into a specially designed PC board and flush mounted to the wall at 4267 mm from the inlet of the channel (Fig. 2(b)), where a fully developed turbulent channel flow exists for the velocity range tested. The experiment was carried out at different Re ($= hu_\infty/\nu$, where h is the half-width of the channel) ranging from 8758 to 17517.

3. Results and discussion

3.1. Shear stress distribution

Fig. 3 shows the contours of 2-D shear stress distribution measured by the 25 sensors covering an area 7.5 mm in width, 20 ms in time for three different Re numbers. Areas of high shear stress are marked by light gray in the plots while dark gray represents low shear stress. Note that the transverse scale of the longitudinal high shear stress streaks varies directly with Re number. At high Re, the streaks are narrower. They also appear to have shorter time length.

3.2. Probability density function of wall shear stress

Based on the fluctuating shear stress data measured during a 2.5 s sampling time at 10 kHz acquisition rate, the probability density functions (PDFs) are calculated and shown in Fig. 4(a). As the Re increases, the peak value of the PDF distribution shifts towards the higher shear stress side, indicating an increase in the time-average shear stress level. The minimum shear stress level also changes with the Re. The PDFs are normalized and compared to those laser gradient meter (LGM) by Obi et al. (1996) at $Re = 3300$ (Fig. 4(b)). The non-dimensional shear stress τ^* is defined as

$$\tau^* = (\tau - \tau_m)/\tau', \tag{6}$$

where τ_m is the time-average shear stress and τ' is the rms of shear stress. The PDFs are normalized so that the integrated

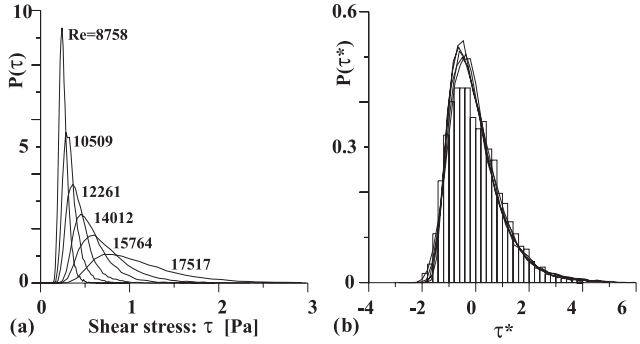

Fig. 4. (a) PDF of shear stress at different Reynolds numbers; (b) normalized PDF: $\tau^* = (\tau - \tau_m)/\tau_{rms}$ solid lines are measured by the micro shear stress sensor and bar chart is from Obi et al. (1996).

volume is unity. All the PDFs overlap one distribution and the distribution agrees very well with the LGM data. The performance of the micro-shear stress sensor is examined by comparing the turbulent statistics measured by the micro-sensor with that of previous experiments and computations. The root mean square, skewness factor and flatness factor of surface shear stress are 0.4, 1.09, and 4.6, respectively. The turbulence statistics measured by the micro-sensor are in good agreement with previous experimental and numerical results Obi et al. (1996).

3.3. High shear stress streaks

To investigate the characteristics of the high shear stress streaks, a threshold of signal level is needed in order to separate the streaks from background fluctuations. This criterion should be able to 'mark' the high shear stress area so that the streaks can be isolated. As τ^* is based on the ratio of the instantaneous 2-D shear stress to the time-average level, it is chosen to be the criterion. The best threshold level of τ^* allowing a shear stress streak to be identified is decided by the two factors. One is the separation between high shear streaks to pick up from the shear stress sensor contour. Fig. 5 shows the change streak areas that are identified according to

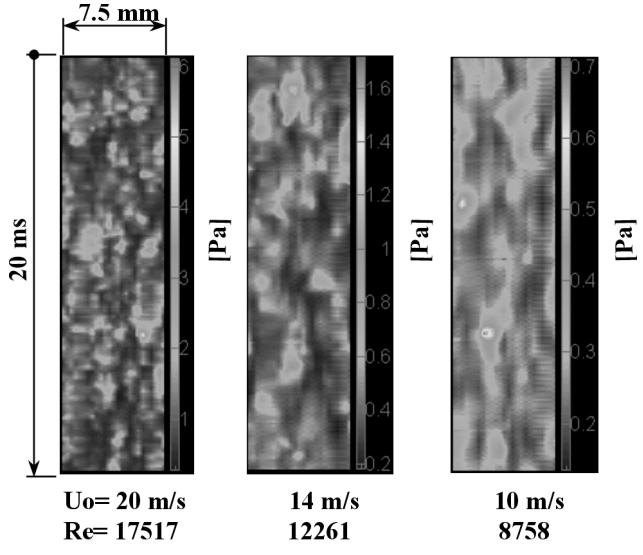

Fig. 3. Instantaneous surface shear stress measured by the imaging chip.

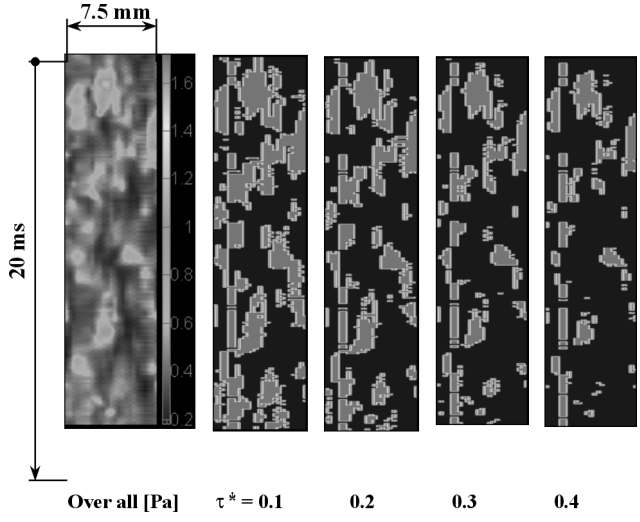

Fig. 5. Change of high shear stress area versus τ^* number.

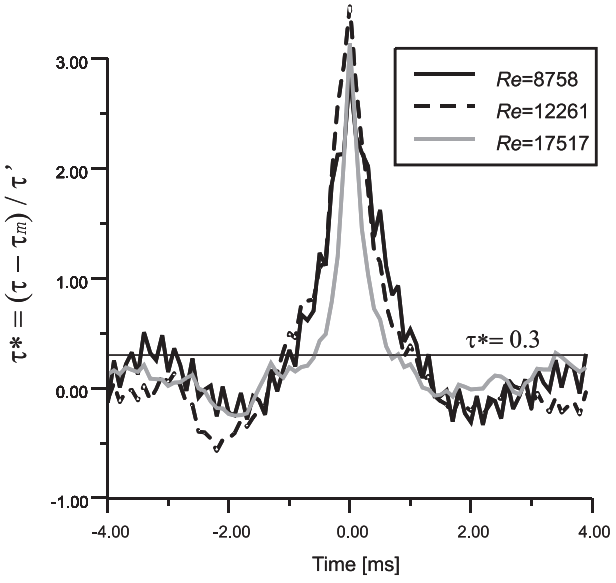

Fig. 6. Ensemble averaged time trace of high shear stress streak and threshold.

different values of τ^*. Areas of high shear stress marked by light gray plots while dark gray represents low shear stress. The area of high shear stress streaks decreases as τ^* number increases. The order is the signal level to distinguish between high shear stress streaks and the background fluctuation.

The low value of τ^* is better to predict high shear stress peak in the early stage of high shear stress streaks. Fig. 6 shows the normalized time trace of the shear stress streaks for different *Re*. The traces are the ensemble averages of the 'Center' trace of shear stress streaks. The sensor that detects the peak shear stress of a streak measures the Center trace. The figure shows that the normalized peak levels of shear stress streaks are similar in spite of the different *Re*. It is determined that a τ^* value of 0.3 is the best threshold level in identifying the structures because of the shear stress streaks separation.

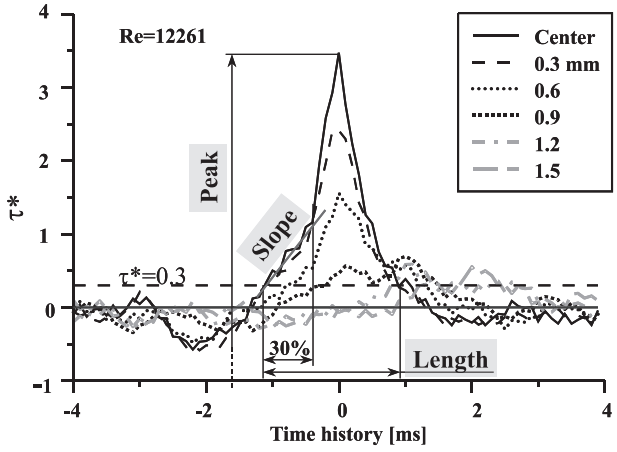

Fig. 7. Peak, length and slope of streak.

3.4. Definition of peak, length and slope of streaks

One of the aims of studying the 2-D shear stress distribution is to develop an identification criterion that can be used by a control logic circuit to detect the passage of the high shear stress streaks. To develop such a criterion, the characteristics of the streaks, length, peak shear stress levels and shear stress slopes are examined.

Peak, length and slope of high shear stress streaks are illustrated in Fig. 7. The peak is defined as the maximum shear stress in the streak. The length defined as the streak length in time of limit above $\tau^* = 0.3$. The threshold $\tau^* = 0.3$ is decided by the area separation of high shear stress streaks to pick up high shear stress streaks, and the background fluctuation level of shear stress as mentioned in Section 3.3. The slope is defined as the front-end (30% of the streak length in time) shear stress gradient of the streak. It is to be desired that the time is as short as possible to predict the peak in early stage. A streak has spread out in 2-D, so that it has several slopes in front-end measured by several sensors. In this way, the slope is maximum-slope in a streak.

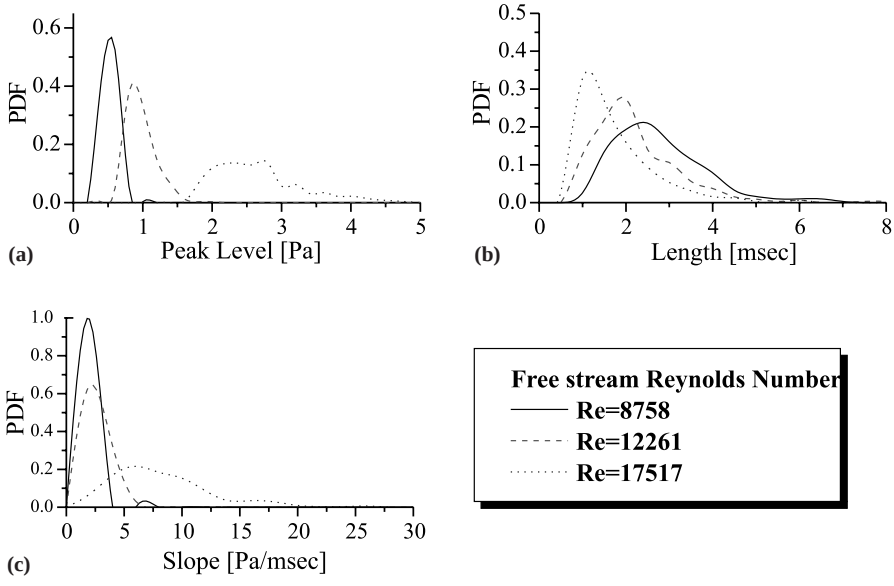

Fig. 8. PDF of characteristics of high shear stress streak.

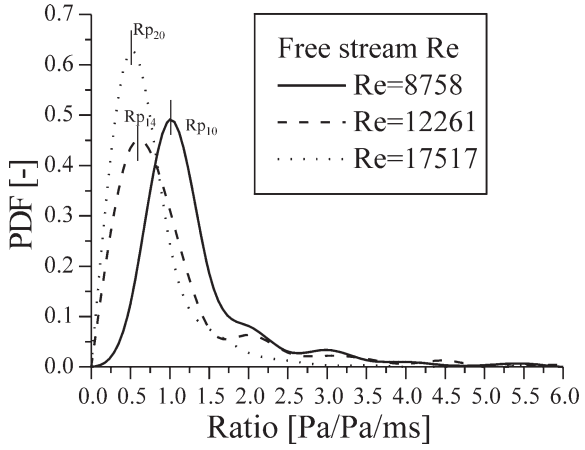

Fig. 9. The ratio of peak shear stress to shear stress gradient at different Re's.

3.5. Statistical characteristics of streaks

Fig. 8 shows the PDFs of several shear stress streaks' characteristics at different *Re*. Fig. 8(a) shows the PDF of the shear stress peak at different *Re* number. As the *Re* increases, the peak average increases from 0.4 to 2.5 Pa, and the distribution becomes wider. Fig. 8(b) shows the PDF of the streak time length at different *Re*. As the *Re* increases, the average streak time length decreases from 2.5 to 1.5 ms, and its distribution becomes narrower. Fig. 8(c) shows the PDF of the shear stress slope. For $Re = 8758$, the slope distribution is concentrated in a small area. As the *Re* increases, the average shear stress slope increases from 2.0 to 7.0 Pa/ms, and the distribution becomes wider.

3.6. Prediction of peak shear stress

To explore the relationship between the shear stress slope and the peak shear stress, the PDFs of the ratio of peak shear stress to shear stress slope at different *Re* are examined. As shown in Fig. 9, the PDF distributions for all *Re* cases have a peak in a narrow range, indicating the existence of a preferred ratio. The peak value of the PDF decreases with increasing *Re* number. The highest probability ratio *Rp* for each *Re* number is 0.5 Pa/Pa/ms ($Re = 17517$), 0.6 Pa/Pa/ms ($Re = 12261$), and 1.0 Pa/Pa/ms ($Re = 8758$), respectively. The ratio range from $Rp - 0.4$ to $Rp + 0.4$ Pa/Pa/ms covers probability of the ratio distribution greater than 60%.

By multiplying this ratio (peak to slope of shear stress at the peak value of the PDF) by the measured front-end slope of individual streaks, we can "predict" the peak value of the shear stress in real-time due to the correlation between the two values. This result is extremely important because it points to the possibility of predicting the peak shear stress level based on the shear stress distribution at the leading edge of the streaks.

4. Conclusion

A micro-machined surface shear stress imaging chip was used to measure the instantaneous shear stress distribution on the wall in a turbulent boundary layer. The statistics associated with near-wall high shear stress streaks were studied. To investigate the characteristic of the high shear stress streaks, we first determined a threshold to separate the streak from the background fluctuation. Several characteristics of the shear stress streaks, such as the length, the width of the front-end slope, and the shear stress peak are obtained at different *Re*.

In particular, reasonable correlation between the peak shear stress and its front-end slope of a streak was established. It was further shown that the ratio of the peak shear stress to the front-end slope of shear stress streaks has sharp peak in its probability density distribution. The peak value of PDF decreases with increasing *Re* number. These two findings are extremely important. By multiplying this ratio (peak to slope of shear stress at the peak value of the PDF) by the measured front-end slope of individual streaks, we can predict the peak value of the shear stress in real-time due to the correlation between the two values. We can then determine the necessary input driving level to the actuator for reducing the shear stress. This result will be implemented in the algorithm for the integrated turbulent boundary layer control system.

Acknowledgements

This work is supported by an URI project from US Air Force Office of Scientific Research. The exchange visitor program UCLA, USA and Nihon University, Japan support M. Kimura. We also appreciate the help from Mr. J. Lew. of UCLA, USA and Mr. J. Hoffelner of University of Linz, Austria.

References

Alfreadsson, P.H., Johnansson, A.V., Haritonidis, J.H., Eckelmann, H., 1988. The fluctuating wall-shear stress and the velocity field in the viscous sublayer. Phys. Fluids 31 (5), 1026–1033.

Bruun, H.H. (Ed.), 1995. Hot-wire Anemometry. Oxford University Press, Oxford, pp. 272–286.

Cantwell, B.J., 1981. Organized motion in turbulent flow. Ann. Rev. Fluid Mech. 13, 457–515.

Falco, R., 1980. The Production of Turbulence near a Wall. AIAA Paper, 80–1356.

Head, M.R., Bandyopadhyay, P., 1981. New aspects of turbulent boundary-layers structure. J. Fluid Mech. 107, 297–338.

Ho, C.M., Tung, S., Tai, Y.C., July 1996. Intarctive control of wall structure by MEMS-based transducers. Advances in Turbulence. In: Proceedings of the Sixth European Turbulence Conference. Lausanne, Switzerland, p. 413.

Ho, C.M., Tung, S., Tai, Y.C., Jiang, F., Tsao, T, 1997. MEMS-a technology for advancements in aerospace engineering. AIAA Paper 97-0545.

Huage, J.B., Tung, S., Ho, C.H., Liu, C., Tai, Y.C., 1996. Improved micro thermal shear-stress sensor. IEEE Trans. Instrum. Meas. 45 (2), 570.

Hussain, A.K.M.F., Reynolds, W.C., 1970. The mechanics of a perturbation wave in turbulent shear flow. Air Force office of Scientific Report 70-1655TR. pp. 29–33.

Jiang, F., Tai, Y.C., Gupta, B., Goodman, R., Tung, S., Huang, J.B., Ho, C.M., 1996. A surface-micromachined shear stress imager. In: Proceedings of the Ninth International IEEE Workshop on MEMS. San Diego, p. 110.

Kim, H.T., Kline, S.J., Reynolds, W.C., 1971. The production of turbulence near a smooth wall in a turbulent boundary layer. J. Fluid Mech. 50, 133–160 (Part 1).

Kim, J., Moin, P., Moser, R., 1987. Turbulant statistics in fully developed channel flow at low Reynolds number. J. Fluid Mech. 177, 133–160.

Kline, S.J., Reynolds, W.C., Schraub, F.A., Runstadler, P.W., 1967. The structure of turbulent boundary layers. J. Fluid Mech. 30, 741–773 (Part 4).

Naqwi, A.A., Reynolds, W.C., 1991. Measurement of turbulent wall velocity gradient using cylindrical waves of laser light. Exp. Fluids 10, 257–266.

Obi, S., Inoue, K., Furukawa, T., Masuda, S., 1996. Experimental study on the statistics of wall shear stress in turbulent channel flows. J. Heat Fluid Flow 17, 187–192.

Smith, C.R., Metzler, S.P., 1983. The characteristics of low-speed streaks in the near-wall region of a turbulent boundary layer. J. Fluid Mech. 129, 27–54.

Tung, S., Hong, H., Huang, J.B., Ho, C.M., Liu, C., Tai, Y.C., August 1995. Control of a streamwise vortex by a mechanical actuator. In: Proceedings of the 10th Symposium on Turbulent Shear Flows, vol. 1. Pennsylvania, USA, pp. 1–19.